

Mechanism of ovaling vibrations of cylindrical shells in cross flow

Yasushi Uematsu[†]

Department of Architecture and Building Science, Tohoku University, Sendai 980-8579, Japan

Noboru Tsujiguchi[‡]

Yokohama Branch, Nishimatsu Construction Co. Ltd., Yokohama, Japan

Motohiko Yamada^{‡†}

New Industry Creation Hatchery Center, Tohoku University, Sendai 980-8579, Japan

Abstract. The mechanism of wind-induced ovaling vibrations of cylindrical shells is numerically investigated by using a vortex method. The subject of this paper is limited to a two-dimensional structure in the subcritical regime. The aerodynamic stability of the ovaling vibrations in the second to fourth circumferential modes is discussed, based on the results of a forced-vibration test. In the analysis, two modal configurations are considered; one is symmetric and the other is anti-symmetric with respect to a diameter parallel to the flow direction. The unsteady pressures acting on a vibrating cylinder are simulated and the work done by them for one cycle of a harmonic motion is computed. The effects of a splitter plate on the flow around the cylinder as well as on the aerodynamic stability of the ovaling vibrations are also discussed. The consideration on the mechanism of ovaling vibrations is verified by the results of a free-vibration test.

Key words: circular cylinder; ovaling vibration; cross flow; numerical simulation; vortex method; unsteady aerodynamic force; two-dimensional.

1. Introduction

Ovaling vibration of cylindrical structures such as chimney stacks refers to the shell-mode vibration, involving deformation of the cross section in a circumferential mode, n , higher than unity. This phenomenon has arisen with the construction of thin metal chimney stacks, which are thin enough to easily deform as shells and have low internal damping. Historically, such vibrations were first observed by Dickey and Woodruff (1956) and Dockstader *et al.* (1956). Johns and Allwood (1968) described a case of large amplitude vibration, which eventually led to a collapse of the chimney during a typhoon. Even if the amplitude is not large enough to collapse the structure, the vibration may cause the structural elements to fail due to fatigue.

[†] Associate Professor

[‡] Engineer

^{‡†} Professor

The ovalling vibrations were originally thought to be excited subharmonically by vortex shedding, such that the ratio of one of the shell's natural frequencies to the vortex shedding frequency is an integer at the onset of ovalling vibration (see Johns and Sharma 1974 and Panesar and Johns 1985). On the other hand, Païdoussis *et al.* (1979, 1982a) experimentally revealed that the existence of regular, periodic vortex shedding is not essential for the onset of ovalling vibrations. They subsequently developed an analytical model for predicting the onset velocity, in which the vibration was regarded as a flutter, drawing energy from the flow in synchronism with its natural motions (1982b, 1988, 1991). In their model, the flow field is considered to be quasi-irrotational and steady, the only unsteadiness being associated with shell motion. Katsura (1985) experimentally studied the ovalling vibrations of silo-like, thin cylindrical shells. Some of his results confirmed the findings of Païdoussis *et al.* He also examined the effect of free-stream turbulence on the characteristics of ovalling vibrations and showed that the ovalling amplitude grew suddenly at a certain flow velocity in a smooth flow, while it increased nearly proportional to the square of the free-stream velocity in a turbulent flow, or to the velocity pressure of the flow. Mazouzi *et al.* (1991) improved the Païdoussis *et al.*'s analytical model, considering the Reynolds number effects on the flow around circular cylinders. Recently, Laneville and Mazouzi (1995, 1996) have proposed a new criterion for the onset of ovalling vibrations, which is based on a balance between the negative aerodynamic damping and the shell's structural damping. Uematsu *et al.* (1988) experimentally studied the ovalling vibrations of finite cylinders with relatively small aspect ratios and proposed an excitation mechanism, based on a cross-spectral density analysis of the pressure fluctuations on the cylinder surface.

As mentioned above, the mechanism of wind-induced ovalling vibrations of cylindrical shells is controversial even for the two-dimensional problem. It may be important for discussing the mechanism to investigate the aerodynamic stability of the vibrations, or the characteristics of the unsteady aerodynamic forces acting on a vibrating cylinder.

In this study, we choose a two-dimensional structure in the subcritical regime as the most fundamental subject. The unsteady pressures acting on a vibrating cylinder are computed by using a vortex method; ovalling vibrations in the second to fourth modes ($n=2-4$) are considered. The aerodynamic stability of these vibrations is discussed, based on the work done by the unsteady pressures for one cycle of a harmonic motion. The effects of a splitter plate on the flow around the cylinder as well as on the aerodynamic stability of the ovalling vibrations are also investigated. Furthermore, in order to verify the consideration on the mechanism of ovalling vibrations, a free-vibration test is made for a cylindrical shell model with or without a splitter plate.

It should be mentioned that the present paper is an extended version of our previous papers (Uematsu *et al.* 1999a, b). The results and discussion are presented in more detail in this paper.

2. Method of numerical simulation

A vortex method developed by Inamuro and Adachi (1986) is applied to the present problem with some revisions. Cylinder surface is divided into a number, M , of segments of equal length and replaced by a continuous vortex sheet. The circulation $\gamma(s)$ per unit length of the vortex sheet changes linearly along the segment, with s being the coordinate along the cylinder surface C ; the value at a node j is represented by γ_j ($j=1-M$). The free shear layers are replaced by discrete vortices shed into the flow field from the separation points at a time step Δt . The circulation Γ of each discrete vortex is given by $(1/2)U_s^2 \Delta t$, with U_s being the velocity of the outer flow at the separation point θ_s . It is assumed that the boundary layer is laminar and the thickness is thin

enough to be neglected. The separation points are determined by solving the boundary layer momentum equation with Pohlhausen's quasi-steady approximation. In the numerical integration of this equation, the cylinder surface is divided into a number, $2M$, of segments. The splitter plate of length L , when placed behind the cylinder, is replaced by a number, K , of sources arranged at equal distances. The strength Q_k of each source is determined so as to cancel out the flow across the source (see Kawai 1990).

The complex velocity potential $f(z)$ at a point z is given by superimposing the components due to the uniform stream (U_∞), the vortex sheet ($\gamma(s)$), the discrete vortices (Γ_k) and the sources (Q_k) as follows:

$$f = U_\infty z - \frac{i}{2\pi} \oint_C \gamma(s) \log\{z - z(s)\} ds - \frac{i}{2\pi} \sum_{k=1}^N \Gamma_k \log(z - z_{wk}) + \frac{1}{2\pi} \sum_{k=1}^K Q_k \log(z - z_{qk}) \quad (1)$$

where N is the number of the discrete vortices; z_{wk} and z_{qk} represent the locations of the discrete vortex Γ_k and the source Q_k , respectively; and $i = \sqrt{-1}$. The conjugate complex velocity \bar{u} at a point z is given by the following equations:

$$\bar{u} = \frac{df}{dz} = U_\infty + S_1^{(1)} \gamma_1 + \sum_{j=2}^M (S_{j-1}^{(2)} + S_j^{(1)}) \gamma_j + S_M^{(2)} \gamma_1 - \frac{i}{2\pi} \sum_{k=1}^N \frac{\Gamma_k}{z - z_{wk}} + \frac{1}{2\pi} \sum_{k=1}^K \frac{Q_k}{z - z_{qk}} \quad (2)$$

$$S_j^{(1)} = \frac{is_j}{2\pi(z_{j+1} - z_j)} \left(-1 + \frac{z_{j+1} - z}{z_{j+1} - z_j} \log \frac{z_{j+1} - z}{z_j - z} \right) \quad (3)$$

$$S_j^{(2)} = \frac{is_j}{2\pi(z_{j+1} - z_j)} \left(1 - \frac{z_j - z}{z_{j+1} - z_j} \log \frac{z_{j+1} - z}{z_j - z} \right) \quad (4)$$

where z_j represents the location of the node j ; and s_j the length of the segment j .

The boundary condition at the midpoint, regarded as the reference point, z_{rl} of each segment l is given by the following equation:

$$\text{Re}[(\bar{u}_{rl} - \bar{w}_{rl}) \cdot n_{rl}] = 0 \quad (5)$$

where u_{rl} and w_{rl} represent the complex velocities of the flow and the shell motion at z_{rl} , respectively; and n_{rl} is the unit normal vector, positive outward, at z_{rl} . An additional equation is given by Kelvin's theorem as follows:

$$\sum_{j=1}^M \frac{s_j}{2} (\gamma_j + \gamma_{j+1}) \sum_{k=1}^N \Gamma_k + 0 \quad (6)$$

From the boundary conditions at z_{rl} ($l = 1-M$) together with Eq. (6), we obtain simultaneous linear equations with respect to γ_j ($j = 1-M$). The equations can be solved by using the least squares method.

The position of the discrete vortices is advanced in a way of simple Eulerian scheme with a time step of $\Delta t/2$. In the region of point vortices, the velocity tends to infinity because of the singular nature of ideal point vortices. This phenomenon is not encountered in a real fluid. Therefore, some type of artificial viscosity is required to compensate such an irregularity. Fig. 1 shows a viscous vortex model (solid lines) used in this study. Outside a viscous core radius σ , the circumferential velocity V_θ is the potential solution; within the core radius, V_θ is proportional to the distance r from the center. The value of σ is given by a function of the coefficient of kinematic viscosity ν of the

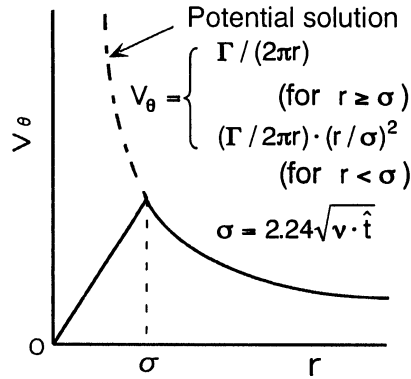


Fig. 1 Viscous vortex model

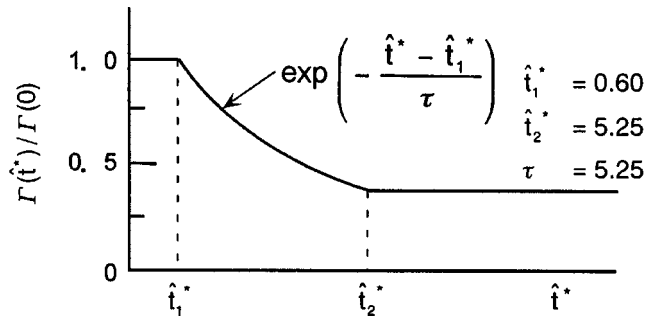


Fig. 2 Circulation reduction model

fluid and the lifetime \hat{t} of the vortex. Furthermore, it has been recognized that some circulation-reduction mechanism is inevitable to obtain reasonable results by the model. Fig. 2 shows a model developed in this study, based on the results of a wind tunnel experiment (Nagano *et al.* 1981) and a preliminary analysis. In the figure, \hat{t}^* represents the non-dimensional lifetime of the vortex, defined by $\hat{t}^* = U_\infty \hat{t} / D$, with D being the cylinder diameter.

The instantaneous pressure $p(\theta, t)$ on the cylinder surface is given by the unsteady Bernoulli's equation :

$$p(\theta, t) - p_\infty = \frac{1}{2} \rho [U_\infty^2 - (u^2 + v^2)] - \rho \frac{\partial \Phi}{\partial t} \tag{7}$$

where θ = angle from the windward stagnation point; p_∞ = pressure at upstream infinity; ρ = fluid density; u and v are the velocity components in the longitudinal and lateral directions, respectively; Φ = velocity potential; and $\partial \Phi / \partial t$ is approximated by a finite difference of the first order. The pressure distribution is expanded into a circumferential Fourier series as follows :

$$p(\theta, t) - p_\infty = \sum_{n=0}^{12} [b_n(t) \cos n\theta + c_n(t) \sin n\theta] \tag{8}$$

The coefficients $b_n(t)$ and $c_n(t)$ are determined by using the least squares method. We can easily compute the modal forces and the work done by the unsteady pressures with this approximation.

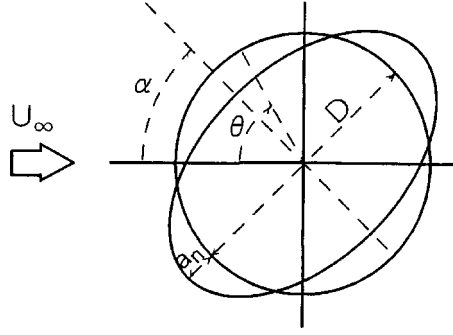


Fig. 3 Cross-sectional view of the mode of ovaling vibration (in the case of $n = 2$)

The pressure coefficient $C_p(\theta, t)$ is defined by $C_p(\theta, t) = (p(\theta, t) - p_\infty) / q_\infty$, with $q_\infty = 1/2 \rho U_\infty^2$.

The mode shape $\phi_n(\theta)$ of the n -th ovaling vibration is expressed as follows (see Fig. 3) :

$$\phi_n(\theta) = \cos n(\theta - \alpha) \quad (9)$$

where α represents the angle of an anti-node of vibration from the windward stagnation point; $\alpha = 0^\circ$ and $90^\circ/n$ respectively correspond to a symmetric and an anti-symmetric mode. The n -th modal force $F_n(t)$ is computed by

$$F_n(t) = \frac{D}{2} \int_0^{2\pi} \{p(\theta, t) - p_\infty\} \phi_n(\theta) d\theta \quad (10)$$

The modal force coefficient $C_{Fn}(t)$ is defined by $C_{Fn}(t) = F_n(t) / (q_\infty D)$.

In the forced-vibration tests, the ovaling vibration is given by the following equation :

$$w(\theta, t) = a_n \sin(2\pi f_m t) \cdot \phi_n(\theta) = a_n \sin(2\pi f_m t) \cdot \cos n(\theta - \alpha) \quad (11)$$

where a_n and f_m are the amplitude and the frequency of the forced vibration, respectively. The work done by $p(\theta, t)$ for one cycle, $T_m (= 1/f_m)$, of the harmonic motion is

$$W = \frac{D}{2} \int_0^{T_m} \left\{ \int_0^{2\pi} \{p(\theta, t) - p_\infty\} \frac{dw}{dt} d\theta \right\} dt \quad (12)$$

The positive and negative values of W are related to the negative and the positive aerodynamic damping, respectively. When $W > 0$, the energy from the unsteady pressures is applied to the shell, and the shell vibration may be amplified. The non-dimensional work W^* is defined by $W^* = W / (1/2 q_\infty D^2)$.

The values of the parameters involved in the simulation model are as follows :

$$M = 80, \Delta t(U_\infty / D) = 0.15, R_e = U_\infty D / \nu = 8 \times 10^4, L/D = 0.25 - 5.0, K = 25 \times (L/D)$$

These values were determined from the results of a preliminary analysis as well as of the previous studies.

In practice, the time development of flow around an impulsively started cylinder is simulated. A transient response is seen when $t^* (= t(U_\infty / D)) < 50$. Therefore, the statistical analysis of the response is made by using the results for $t^* = 75 - 150$.

3. Aerodynamic forces

3.1. Steady aerodynamic forces acting on a stationary cylinder

3.1.1. Cylinder without a splitter plate

Fig. 4 shows sample results on the instantaneous flow pattern around a stationary cylinder. In order to verify the simulation model used in this study, a comparison was made between the present analysis and a wind tunnel experiment (Fage and Falkner 1931, quoted from Roshko 1961) for the aerodynamic properties. The result for the mean pressure coefficient \bar{C}_p is shown in Fig. 5. Table 1 summarizes the results for the aerodynamic properties, together with some available experimental results obtained at $Re \approx 8 \times 10^4$. The agreement is generally good, confirming the validity of the simulation model.

The mean and RMS values of the modal force coefficients $C_{Fn}(t)$ ($n = 2-4$) are plotted against α in Fig. 6. The mean value becomes the maximum when $\alpha = 0^\circ$ and the minimum when $\alpha = 90^\circ/n$. This feature is expected from a symmetric distribution of \bar{C}_p with respect to a diameter parallel to the flow direction. The results for the RMS value show the opposite trend. The power spectra S_n of $C_{Fn}(t)$ ($n = 2-4$) are shown in Fig. 7. The solid and broken lines represent the results for the symmetric and anti-symmetric modes, respectively. The power spectra for the anti-symmetric modes

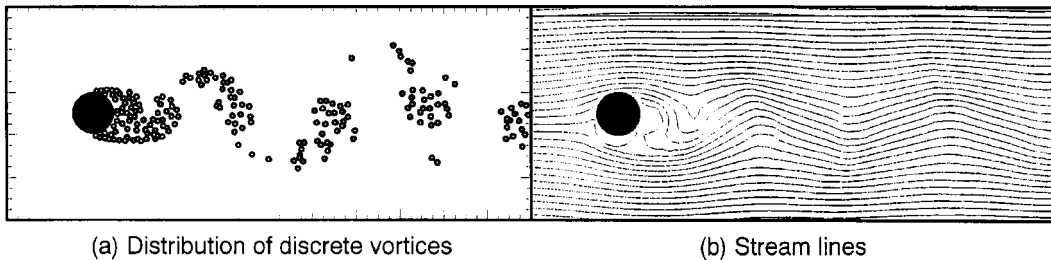


Fig. 4 Instantaneous flow pattern around a stationary cylinder at $t^* = 150$

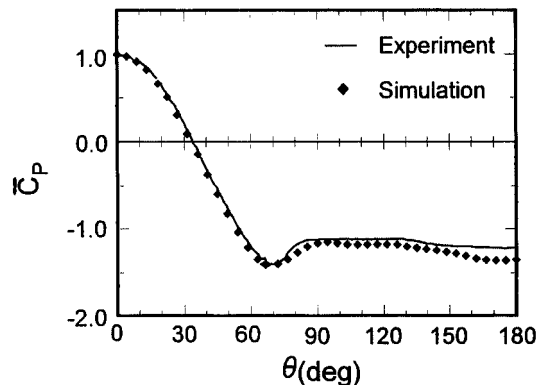
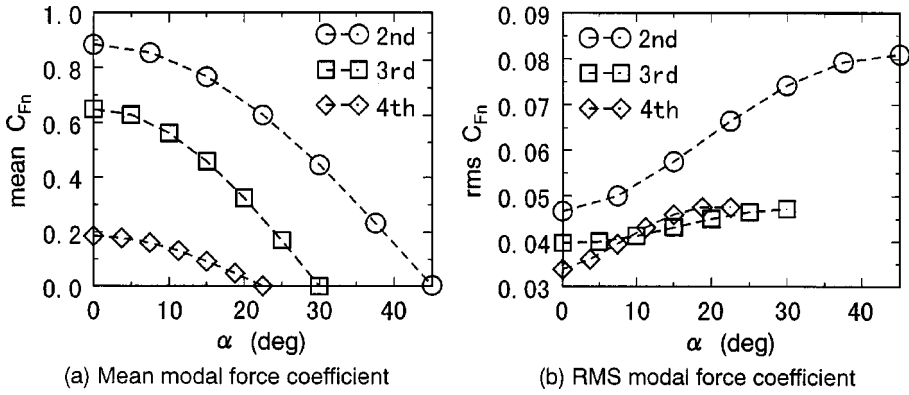
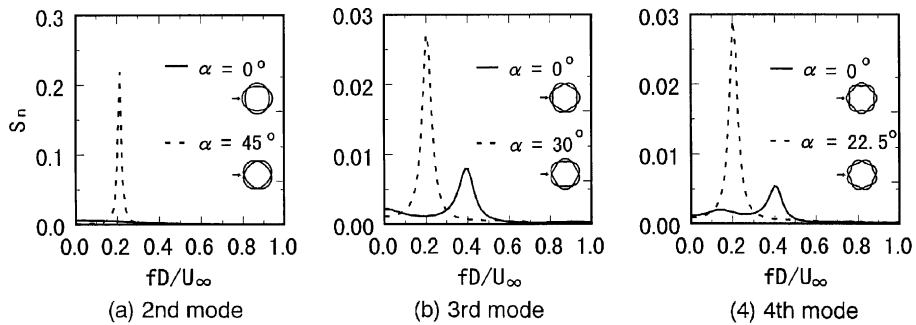


Fig. 5 Comparison between simulation and experiment for the circumferential distribution of the mean pressure coefficient \bar{C}_p

Table 1 Comparison of the computed results with the experimental results

Aerodynamics	Present analysis	Experiment	Reference
Drag coefficient C_D	1.26	1.2 ($R_e = 8 \times 10^4$) 1.2 ($R_e = 8 \times 10^4$)	Wieselsberger (1921) Schewe (1983)
RMS lift coefficient C_L'	0.51	0.32 ($R_e = 8 \times 10^4$) 0.55 ($R_e = 9 \times 10^4$) 0.56 ($R_e = 6 \times 10^4$)	Schewe (1983) West & Apelt (1993) Nishimura & Taniike (1998)
Strouhal number S_t	0.209	0.19 ($R_e = 8 \times 10^4$) 0.20 ($R_e = 8 \times 10^4$)	Relf & Simmons (1924) Schewe (1983)
Separation point θ_s	81.1°	78° ($R_e = 1 \times 10^5$) 80° ($R_e = 9 \times 10^4$) 82° ($R_e = 8 \times 10^4$)	Achenbach (1968) Adachi <i>et al.</i> (1985) Yamada <i>et al.</i> (1988)


 Fig. 6 Mean and RMS values of the modal force coefficients $C_{Fn}(t)$

 Fig. 7 Power spectra of the modal force coefficients $C_{Fn}(t)$

generally exhibit predominant peaks at a non-dimensional frequency f^* ($=fD/U_\infty$) approximately equal to the Strouhal number S_t . The power spectra for the third and fourth symmetric modes have peaks at $f^* \approx 0.4$, nearly equal to $2S_t$. These results imply that with an increase in the non-dimensional flow velocity U_n^* ($=U_\infty/f_n D$), the vibrations in the anti-symmetric modes ($n=2-4$) are excited at $U_n^* \approx 1/S_t$, while those in the symmetric modes ($n=3, 4$) at $U_n^* \approx 1/(2S_t)$. However, it

should be noticed that this prediction is based on a vortex-shedding hypothesis, in which the ovalling vibration is regarded as a kind of forced vibration without any consideration of the flow-shell interaction.

3.1.2. Cylinder with a splitter plate

The results for cylinders with a splitter plate are shown in Figs. 8~11. With an increase in the length L of the splitter plate, the magnitude of the base pressure coefficient decreases (see Fig. 9).

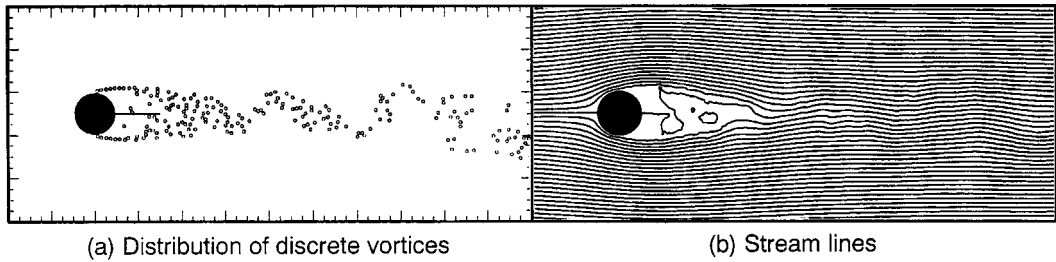


Fig. 8 Instantaneous flow pattern around a stationary cylinder with a splitter plate of $L = D$ at $t^* = 150$

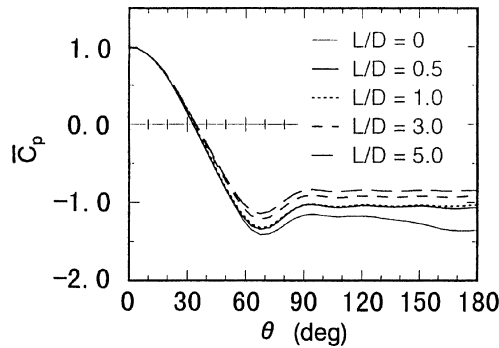


Fig. 9 Effect of L on the circumferential distribution of the mean pressure coefficient \bar{C}_p

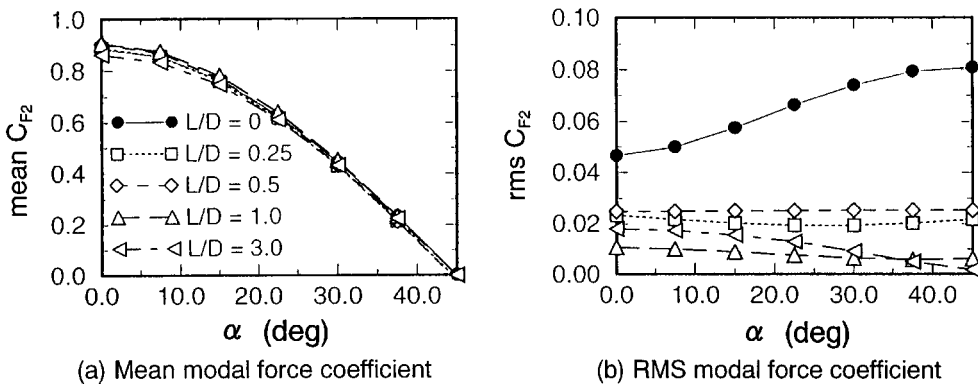


Fig. 10 Effect of L on the mean and RMS values of the second modal force coefficients $C_{F2}(t)$

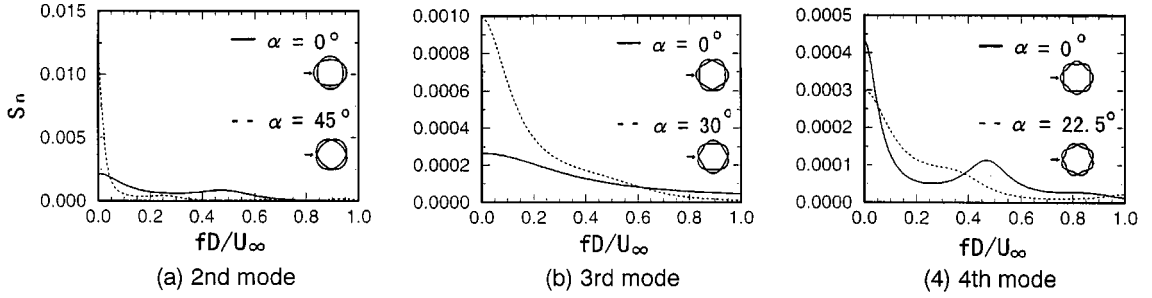


Fig. 11 Power spectra of the modal force coefficients $C_{Fn}(t)$ on a stationary cylinder with a splitter plate of $L = D$

However, this change minutely affects the mean values of the modal force coefficients $C_{Fn}(t)$, as shown in Fig. 10a. On the other hand, the influence on the fluctuation of the modal force coefficient is significant. The RMS value of $C_{Fn}(t)$ becomes small, even when a splitter plate is as short as $L = 0.25D$ (see Fig. 10b). Corresponding to this feature, the power spectra of $C_{Fn}(t)$ exhibit peaks neither at $f^* = S_t$ nor at $f^* = 2S_t$, as shown in Fig. 11.

3.2. Unsteady aerodynamic forces acting on a vibrating cylinder

3.2.1. Cylinder without a splitter plate

The cylinder is forced to vibrate in either a symmetric or an anti-symmetric mode. The non-dimensional amplitude a_n^* ($= a_n/D$) and frequency f_m^* ($= f_m D/U_\infty$) are varied from 0.00125 to 0.01 and from 0.12 to 0.80, respectively. Fig. 12 shows the variation of the power spectra S_2 of the second modal force coefficient $C_{F2}(t)$ with an increase in f_m^* for $a_m^* = 0.00125$ and 0.01. When the amplitude is small (e.g., Fig. 12a), the spectrum for the anti-symmetric mode (broken line) has a peak at $f^* \approx 0.21$ ($= S_t$) regardless of f_m^* ; in particular, the peak is predominant when $f_m^* = 0.20$ ($\approx S_t$). On the other hand, the spectrum for the symmetric mode (solid line) is generally dominated by low-frequency fluctuations, which may be related to the randomness of the flow around the cylinder.

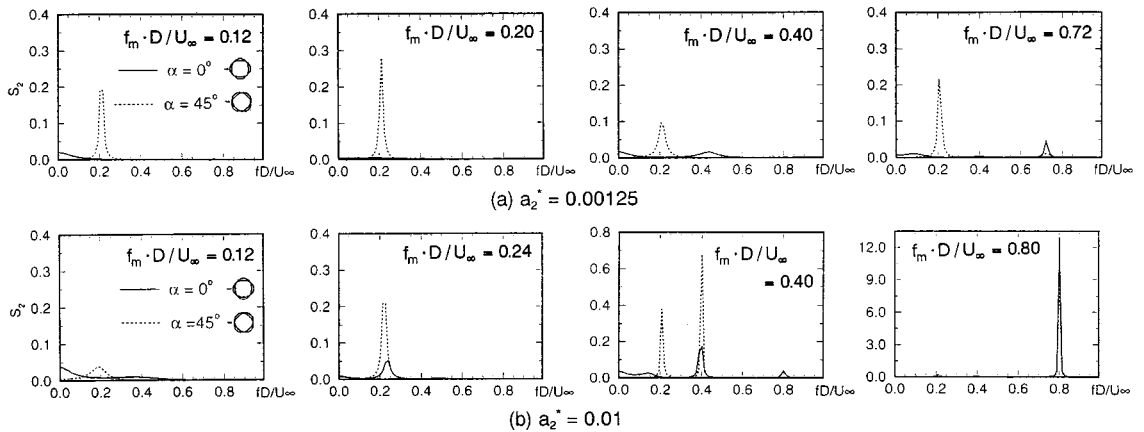


Fig. 12 Power spectra of the second modal force coefficient $C_{F2}(t)$ on a vibrating cylinder

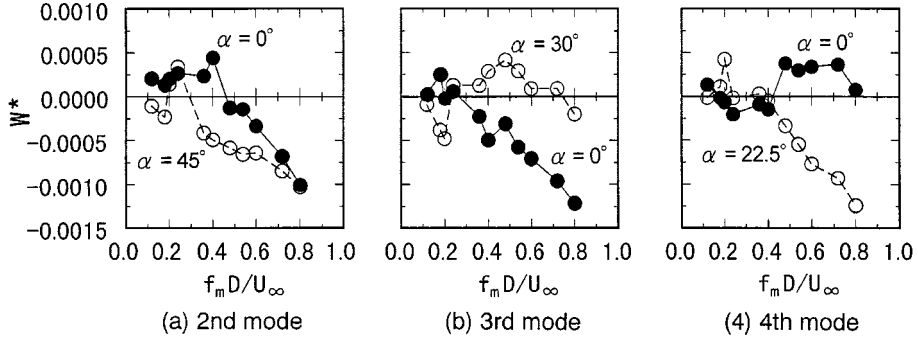


Fig. 13 Variation of W^* with f_m^* for a vibrating cylinder ($a_n^* = 0.005$)

Table 2 Non-dimensional frequency range giving positive W^* values

Mode	Symmetric	Anti-symmetric
2nd	$< 2S_t$	$\approx S_t$
3rd	$\approx S_t$	$S_t - 3S_t$
4th	$2S_t - 4S_t$	$\approx S_t$

The spectral peak due to the forced vibration can be seen only when f_m^* is relatively high, for example, such as $f_m^* > 0.4$. As the amplitude becomes large (e.g., $a_n^* > 0.005$), the spectral peak at $f^* = f_m^*$ becomes predominant for both symmetric and anti-symmetric modes. When $f_m^* = 0.4$, the spectrum for the anti-symmetric mode has predominant peaks both at $f^* \approx 0.2 (\approx S_t)$ and at $f^* \approx 0.4 (\approx 2S_t)$ (see Fig. 12b). The results for the third and fourth modal forces, $F_3(t)$ and $F_4(t)$, not shown in this paper, were similar to those for the second modal force $F_2(t)$.

Plotted in Fig. 13 is the variation of the non-dimensional work W^* with f_m^* in the case of $a_n^* = 0.005$ ($n = 2-4$); the behavior of W^* for the other a_n^* values was almost the same as that shown in this figure, although the values of W^* depended on a_n^* . The non-dimensional frequency range, giving positive W^* values (i.e., negative aerodynamic damping), are summarized in Table 2. Regarding the second mode vibration, for example, the value of W^* becomes positive in a non-dimensional frequency range around $f_m^* = S_t$ for the anti-symmetric mode ($\alpha = 45^\circ$) and in a range of $f_m^* < 2S_t$ for the symmetric mode ($\alpha = 0^\circ$). These features are consistent with the variation of the power spectra of $F_2(t)$ with f_m^* (Fig. 12). Based on these results, the behavior of the second mode vibration with an increase in $U_2^* (= U_\infty / f_2 D)$, or with a decrease in $f_2^* (= f_2 D / U_\infty)$, may be predicted as follows. Self-excited vibrations in the symmetric and anti-symmetric modes occur at $U_2^* \approx 1/(2S_t)$ and $U_2^* \approx 1/S_t$, respectively. The prediction for the symmetric mode is in accordance with the experimental result by Paidoussis *et al.* (1979), who showed that a divergence-type vibration in the symmetric mode occurred at $U_2^* \approx 1/(2S_t)$. In their experiment, the onset non-dimensional flow velocity for the anti-symmetric mode was $U_2^* \approx 1/(4S_t)$, lower than the prediction from the present study (i.e., $U_2^* = 1/S_t$). However, the observed vibration subsided after reaching a maximum at a flow velocity; in other words, the vibration was excited only in a limited range of flow velocity. In this flow velocity range, W^* is negative according to the present results (Fig. 13). Furthermore, the power spectrum exhibits a predominant peak at $f^* \approx 0.8 (\approx 4S_t)$, when $f_m^* = 0.8$ (see Fig. 12). These results imply that the vibration induced at $U_2^* \approx 1/(4S_t)$ can be explained by the subharmonic excitation mechanism, as

Johns *et al.* (1974) suggested.

3.2.2. Cylinder with a splitter plate

Fig. 14 shows sample results on the power spectra S_2 of $C_{F2}(t)$ acting on a vibrating cylinder ($a_2^* = 0.005$) with a splitter plate of $L = 3D$. In the power spectra, any Strouhal components are not seen, only the f_m -component being predominant; this is due to the suppression of the periodic vortex shedding (see Fig. 11).

The variation of W^* with f_m^* is plotted in Fig. 15. Comparing the results with those in Fig. 13, it can be seen that the splitter plate affects the behavior of W^* only slightly. When the splitter plate is placed behind the cylinder, the value of W^* for the second anti-symmetric mode ($\alpha = 45^\circ$) is negative over the whole non-dimensional frequency range analyzed; a positive peak of W^* observed at $f_m^* \approx S_t$ in the no splitter plate case disappears. This is the case for the third symmetric mode ($\alpha = 0^\circ$) and for the fourth anti-symmetric mode ($\alpha = 22.5^\circ$). These results suggest that the negative aerodynamic damping at $f_m^* \approx S_t$, observed in the no splitter plate case (see Fig. 13), is related to the vortex shedding. Furthermore, it is found that self-excited vibrations in the second, third and fourth modes can occur at non-dimensional flow velocities of approximately $1/(2S_t)$, $1/(3S_t)$ and $1/(4S_t)$, respectively, as the flow velocity is increased. Considering that the vortex shedding is suppressed by

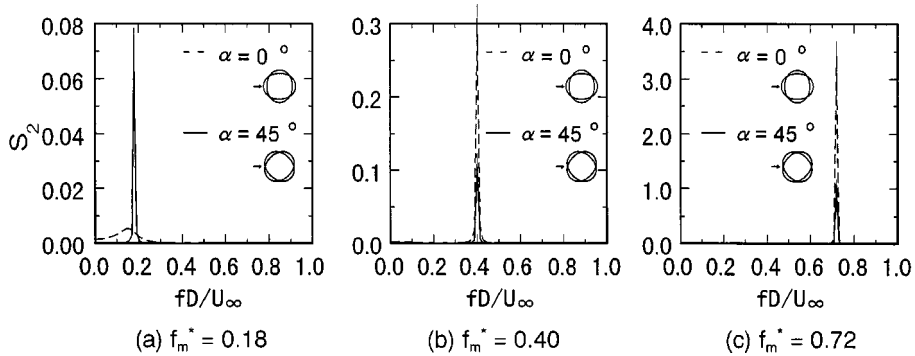


Fig. 14 Power spectra of the second modal force coefficient $C_{F2}(t)$ for a vibrating cylinder ($a_2^* = 0.005$) with a splitter plate of $L = 3D$

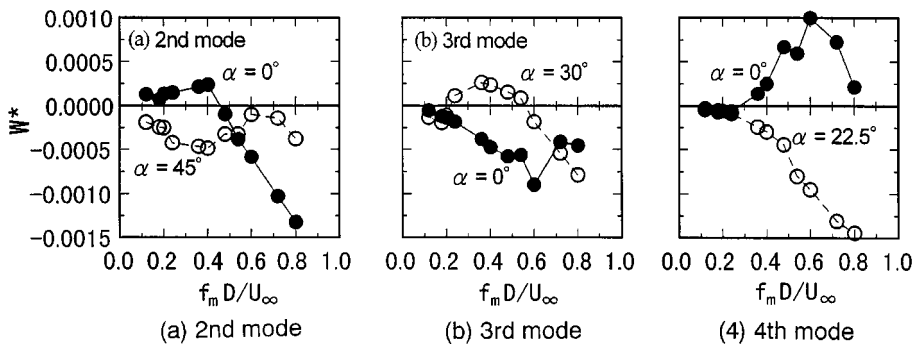


Fig. 15 Variation of W^* with f_m^* for a vibrating cylinder ($a_n^* = 0.005$) with a splitter plate of $L = 3D$

the splitter plate (Fig. 11), it is thought that these vibrations are not related to the vortex shedding.

4. Dynamic response of a shell model

4.1. Method of analysis

The consideration is limited to small-amplitude vibrations, as the first approximation. The shell is considered to be purely elastic, homogeneous and isotropic. Taking the coordinate system as shown in Fig. 16, the basic equations governing the motion of a shell of density ρ_s , Young's modulus E , and Poisson's ratio ν , may be given by the following equations (see Flügge 1957) :

$$\frac{\partial^2 v}{\partial \theta^2} + \frac{\partial w}{\partial \theta} = C_v \frac{\partial v}{\partial t} + \gamma \frac{\partial^2 v}{\partial t^2} \quad (13)$$

$$\frac{\partial v}{\partial \theta} + w + \kappa \left(\frac{\partial^4 w}{\partial \theta^4} + 2 \frac{\partial^2 w}{\partial \theta^2} + w \right) = -C_w \frac{\partial w}{\partial t} - \gamma \left(\frac{\partial^2 w}{\partial t^2} - \frac{q_r}{\rho_s h} \right) \quad (14)$$

where $\kappa = h^2/12a^2$; $\gamma = \rho_s a^2(1-\nu^2)/E$; $q_r = p_i - p_e$, with p_i and p_e being respectively the internal and external pressures acting on the shell surface; and C_v and C_w represent the damping coefficients with respect to the displacements v and w , respectively. Since the internal volume does not change during an ovaling vibration, it is assumed that $p_i = 0$. The external pressure is computed in the same manner as that described in Chapter 2. The effect of the flow-shell interaction is not represented in the equations explicitly, but it is involved in the process of the numerical simulation.

The displacements, v and w , are approximated by the following equations:

$$v(\theta, t) = \sum_{n=2}^N [A_n(t) \cos n\theta + B_n(t) \sin n\theta] \quad (15)$$

$$w(\theta, t) = \sum_{n=2}^N [C_n(t) \cos n\theta + D_n(t) \sin n\theta] \quad (16)$$

Substituting Eqs. (15) and (16) into Eqs. (13) and (14) and applying the Galerkin method to them, we obtain simultaneous coupled equations with respect to the coefficients $A_n(t)$ to $D_n(t)$. The equations are numerically solved by using the Newmark β method with $\beta = 1/4$.

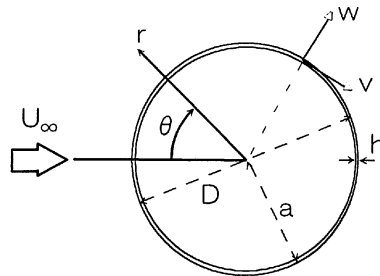


Fig. 16 Shell geometry and coordinate system

4.2. Results of analysis

The properties of a shell model analyzed in this study are as follows :

$$D = 76.2 \text{ mm}, h = 0.483 \text{ mm}, \rho_s = 1.29 \times 10^3 \text{ kg/m}^3, E = 0.28 \times 10^{10} \text{ N/m}^2, \nu = 0.4.$$

These values are the same as those of a clamped-clamped cylinder tested by Païdoussis *et al.* (1982a). The second and third natural frequencies of the present model are 65.9 and 186.5 Hz, respectively. These natural frequencies are different from those of the Païdoussis *et al.*'s specimen, because of the difference in the boundary condition.

Fig. 17(a) shows the time history response of $C_2(t)$ and $D_2(t)$ for an undamped system ($C_v = C_w = 0$) when $U_\infty = 20$ m/s, i.e., $U_\infty/f_2D = 4.0$; in the figure, $t = 0$ represents the time when the free vibration test is started. The corresponding non-dimensional frequency f_2^* is 0.25, which gives positive W^* values both for the symmetric and anti-symmetric modes, according to the results of the forced-vibration test (see Fig. 13). It is seen that the vibration in the symmetric mode ($C_2(t)$) grows with time t . Plotted in Fig. 17(b) are the RMS values of $C_2(t)$ and $D_2(t)$, computed from the responses in a range of t^* ($= tU_\infty/D$) from 15 to 100, as a function of U_2^* ($= U_\infty/f_2D$). Fig. 18 shows the power spectra of $C_2(t)$ and $D_2(t)$, normalized by h , for various values of U_2^* . From the results in Fig. 17(b), it is found that the non-dimensional onset velocities for the symmetric and anti-symmetric modes are approximately 2.5 and 3.5, respectively. These values correspond well to the predicted values from the results in Fig. 13, showing that the sign of W^* becomes positive at $f_m^* \approx 0.4$ and 0.3 for the symmetric and anti-symmetric modes, respectively, as the value of f_m^* decreases. At $U_2^* = 5.0$ (i.e., $f_2^* = 0.2$), the power spectra exhibit predominant peaks at $f^* \approx 0.2$ ($\approx S_1$).

Fig. 19 shows the results for a slightly damped system when $U_\infty = 20$ m/s; the critical damping ratio η_2 of this model is assumed to be 0.001. Comparing the results in Fig. 17, we can see that only a little structural damping reduces the vibration amplitude significantly. In this study, the critical damping ratio η_2 is determined from the uncoupled equations for $A_2(t)$ to $D_2(t)$, obtained by neglecting the coupling terms in the simultaneous equations. Such a manner to determine the structural

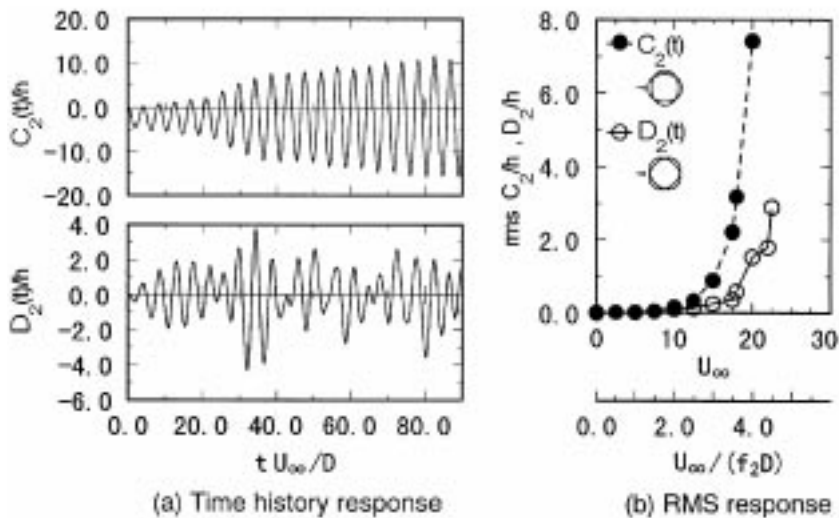


Fig. 17 Responses of $C_2(t)$ and $D_2(t)$ in the no splitter plate case ($\eta_2 = 0$)

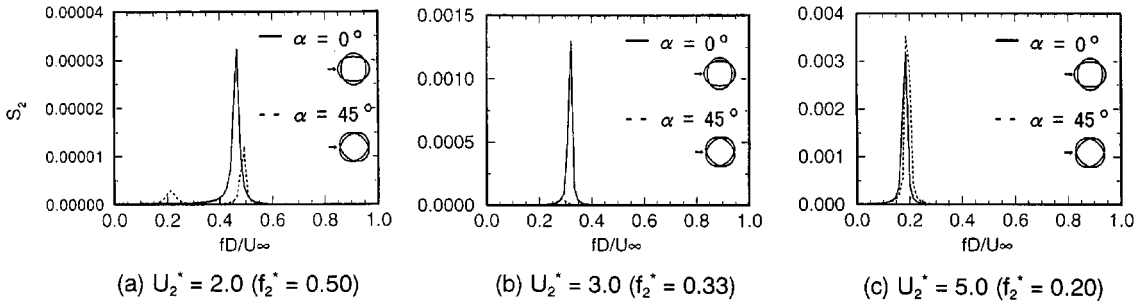


Fig. 18 Power spectra of $C_2(t)$ and $D_2(t)$ in the no splitter plate case ($\eta_2 = 0$)

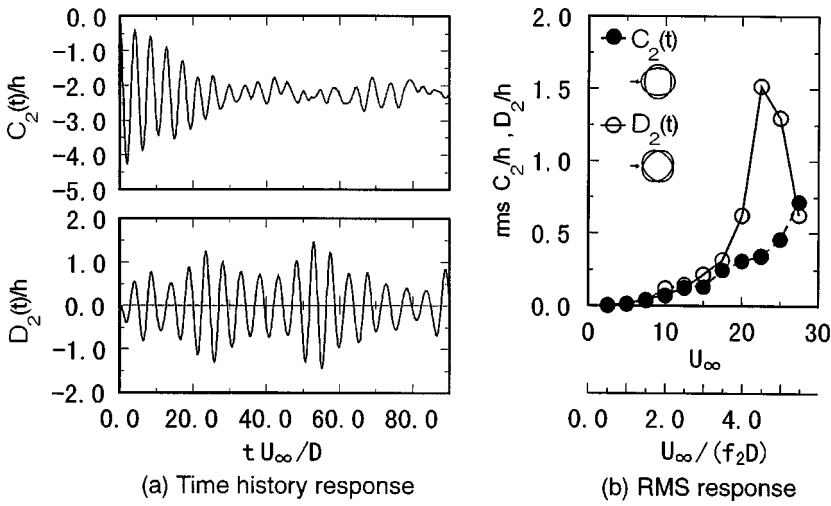


Fig. 19 Responses of $C_2(t)$ and $D_2(t)$ in the no splitter plate case ($\eta_2 = 0.001$)

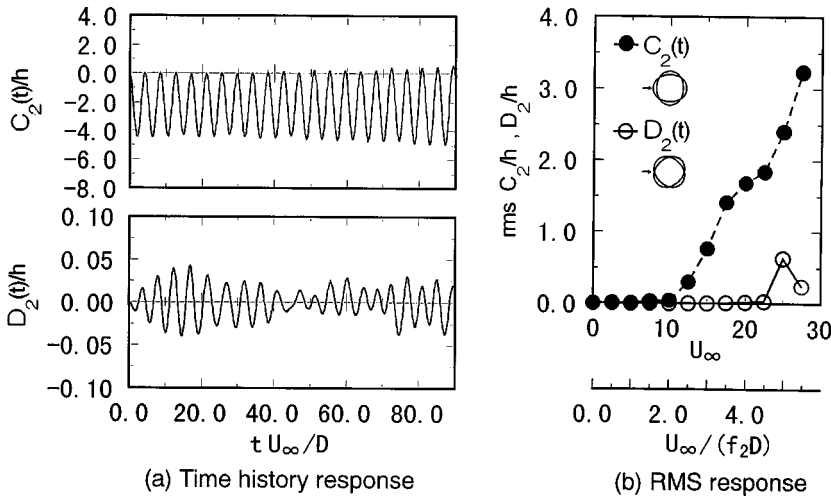


Fig. 20 Responses of $C_2(t)$ and $D_2(t)$ for a cylinder with a splitter plate of $L = 3D$ ($\eta_2 = 0$)

damping is still controversial; this is the subject of a future investigation.

The results for a cylinder with a splitter plate of $L = 3D$ are shown in Fig. 20, in which it is assumed that $\eta_2 = 0$. The vibration in the symmetric mode is excited at $U_2^* \approx 2.5$ in the same manner as that for the no splitter plate case. On the other hand, the vibration in the anti-symmetric mode is rather suppressed. These features are consistent with the expectation from the result for W^* (Fig. 15).

5. Conclusions

The mechanism of wind-induced ovaling vibrations of cylindrical shells has been investigated, based on a numerical simulation of the unsteady aerodynamic forces acting on a vibrating cylinder by using a vortex method. First, a comparison was made between the present analysis and a wind tunnel experiment for the aerodynamics of a stationary cylinder. A good agreement was obtained, suggesting the validity of the simulation model used in this study. Then, the second to fourth modal forces acting on a vibrating cylinder were computed under various conditions. The results indicate that the characteristics of the unsteady aerodynamic forces are related to the vortex shedding from the cylinder. The aerodynamic stability of the ovaling vibrations in the second to fourth modes was investigated, based on the work done by the unsteady pressures for one cycle of a harmonic motion. The vortex shedding may cause self-excited vibrations in a flow velocity range near the resonant velocity for some mode configurations; i.e., the second anti-symmetric, the third symmetric and the fourth anti-symmetric mode. It may be interesting to note that the suppression of vortex shedding by using a splitter plate minutely affects the behavior of the work for some mode configurations; i.e., the second symmetric, the third anti-symmetric and the fourth symmetric mode. Even if the vortex shedding is suppressed by a splitter plate, self-excited vibrations in these modes may occur at some flow velocities, as the flow velocity is increased. In other words, the existence of periodic vortex shedding is not essential for the onset of ovaling vibrations in these modes. These features are consistent with the experimental observations presented by Johns and Sharma (1974) and by Paidoussis and Helleur (1979) to some degree. Finally, the dynamic response of a cylindrical shell model was numerically simulated. The results are consistent with the expectation from the results of the forced vibration tests; this implies the validity of the consideration on the mechanism of the ovaling vibrations.

There are some problems to be solved, regarding the application and accuracy of the simulation model used in this study. Further investigations, including a forced vibration test in a wind tunnel, are planned in order to investigate these problems as well as to discuss the mechanism of ovaling vibrations in more detail.

The authors gratefully acknowledge helpful discussion with Prof. H. Shirato of Kyoto University during this work.

References

- Achenbach, E. (1968), "Distribution of local pressure and skin friction around a circular cylinder in cross-flow up to $Re = 5 \times 10^6$ ", *J. Fluid Mech.*, **34**(4), 625-639.
- Adachi, T., Matsuuchi, K., Matsuda, S. and Kawai, T. (1985), "On the force and vortex shedding on a circular cylinder from subcritical up to transcritical Reynolds numbers", *Trans. Japan Soc. Mech. Engrs. B*, **51**(461), 295-299.
- Dickey, W.L. and Woodruff, G.B. (1956), "The vibrations of steel stacks", *Trans. ASCE*, **121**, 1054-1071.
- Dockstader, E.A., Swinger, W.F. and Ireland, E. (1956), "Resonant vibration of steel stacks", *Trans. ASCE*, **121**, 1088-1112.
- Fage, A. and Falkner, V.M. (1931), "The flow around a circular cylinder", *Aero. Res. Council, Lond., Rep. and*

- Mem., No.1369.
- Flügge, W. (1957), *Statik und Dynamik der Schalen*, 2nd edn. Springer.
- Inamuro, T. and Adachi, T. (1986), "A numerical analysis of unsteady separated flow by vortex shedding model (2nd report, Flow around a circular cylinder)", *Trans. Japan Soc. Mech. Engrs. B*, **52**(476), 1600-1607.
- Johns, D.J. and Allwood, R.J. (1968), "Wind induced ovaling oscillations of circular cylindrical shell structures such as chimneys", *Proc. Symposium on Wind Effects on Buildings and Structures*, Paper 28.
- Johns, D.J. and Sharma, C.B. (1974), "On the mechanism of wind-excited ovaling vibrations of thin circular cylindrical shells", *Flow-Induced Structural Vibrations*, Springer-Verlag, 650-662.
- Katsura, S. (1985), "Wind-excited ovaling vibration of a thin circular cylindrical shell", *J. Sound Vib.*, **100**(4), 527-550.
- Kawai, H. (1990), "Discrete vortex simulation for flow around a circular cylinder with a splitter plate", *J. Wind Eng. Ind. Aerodyn.*, **33**, 153-160.
- Laneville, A. and Mazouzi, A. (1995), "Ovaling oscillations of cantilevered cylindrical shells in cross-flow: new experimental data", *J. Fluids and Structures*, **9**, 729-745.
- Laneville, A. and Mazouzi, A. (1996), "Wind-induced ovaling oscillations of cylindrical shells: critical onset velocity and mode prediction", *J. Fluids and Structures*, **10**, 691-704.
- Mazouzi, A., Laneville, A. and Vittecoq, P. (1991), "An analytical model of the ovaling oscillations of clamped-free and clamped-clamped cylindrical shells in cross-flow", *J. Fluids and Structures*, **5**, 605-626.
- Nagano, S., Naito, M. and Takata, H. (1981), "A numerical analysis of two-dimensional flow past rectangular prisms by a discrete vortex model", *Trans. Japan Soc. Mech. Engrs. B*, **47**(413), 32-43.
- Nishimura, H. and Taniike, Y. (1998), "The mechanism of the occurrence for the fluctuating force on a stationary two-dimensional circular cylinder", *J. Wind Eng., JAWE*, **74**, 47-57.
- Païdoussis, M.P. and Helleur, C. (1979), "On ovaling oscillations of cylindrical shells in cross-flow", *J. Sound and Vibration*, **63**(4), 527-542.
- Païdoussis, M.P., Price, S.J. and Suen, H.-C. (1982a), "Ovaling oscillations of cantilevered and clamped-clamped cylindrical shells in cross flow: an experimental study", *J. Sound and Vibration*, **83**(4), 533-553.
- Païdoussis, M.P., Price, S.J. and Suen, H.-C. (1982b), "An analytical model for ovaling oscillation of clamped-clamped cylindrical shells in cross flow", *J. Sound and Vibration*, **83**(4), 555-572.
- Païdoussis, M.P., Price, S.J. and Ang, S.-Y. (1988), "Ovaling oscillations of cylindrical shells in cross-flow: a review and some new results", *J. Fluids and Structures*, **2**, 95-112.
- Païdoussis, M.P., Price, S.J. and Ang, S.-Y. (1991), "An improved theory for flutter of cylindrical shells in cross-flow", *J. Sound and Vibration*, **149**(2), 197-218.
- Panesar, A. and Johns, D.J. (1985), "Ovaling oscillations of thin circular cylindrical shells in cross flow – an experimental study", *J. Sound and Vibration*, **103**(2), 201-209.
- Relf, E.F. and Simmons, L.F.G. (1924), "The frequency of eddies generated by the motion of circular cylinders through a fluid", *Aero. Res. Council, Lond., Rep. and Mem.*, No.917.
- Roshko, A. (1961), "Experiments on the flow past a circular cylinder at very high Reynolds number", *J. Fluid Mech.*, **10**, 345-356.
- Schewe, G. (1983), "On the force fluctuations acting on a circular cylinder in crossflow from subcritical up to transcritical Reynolds numbers", *J. Fluid Mech.*, **133**, 265-285.
- Uematsu, Y., Uchiyama, K., Yamada, M. and Sanjyo, S. (1988), "Ovaling oscillations of thin circular cylindrical shells in a cross flow", *J. Fluids and Structures*, **2**, 285-307.
- Uematsu, Y., Tsujiguchi, N. and Yamada, M. (1999a), "Numerical investigation of the mechanism for wind-induced ovaling vibrations of thin circular cylindrical structures using vortex method", *J. Struct. Constr. Eng., Architectural Institute of Japan*, **519**, 29-34.
- Uematsu, Y., Tsujiguchi, N. and Yamada, M. (1999b), "Mechanism of ovaling vibrations of cylindrical shells in cross flow", *Proc. 10th Int. Conf. Wind Eng.*, Copenhagen, Denmark, 21-24 June 1999, **2**, 1353-1358.
- Wieselsberger, C. (1921), "Neuere Feststellungen über die Gesetze des Flüssigkeits und Luftwiderstands", *Phys. Z.*, **22**, 321-328.
- West, G.S. and Apelt, C.J. (1993), "Measurements of fluctuating pressures and forces on a circular cylinder in the Reynolds number range 10^4 to 2.5×10^5 ", *J. Fluids and Structures*, **7**, 227-244.
- Yamada, M., Uematsu, Y. and Koshihara, T. (1988), "Visualization of the flow around a two-dimensional circular cylinder by means of infrared thermography (Part 1 smooth cylinder)", *J. Wind Eng., JAWE*, **35**, 35-44.